Steel and Composite Structures, *Vol. 23, No. 1 (2017) 67-85*
DOI: https://doi.org/10.12989/scs.2017.23.1.067

Numerical analysis of tilted angle shear connectors in steel-concrete composite systems

Koosha Khorramian [1], Shervin Maleki [1], Mahdi Shariati [*2], Abdolrahim Jalali [2] and M.M. Tahir [3]

[1] *Department of Civil Engineering, Sharif University of Technology, Tehran, Iran*
[2] *Faculty of Civil Engineering, University of Tabriz, Tabriz, Iran*
[3] *UTM Construction Research Centre, Faculty of Civil Engineering, Institute for Smart Infrastructure and Innovative Construction, UTM, 81310, Johor Bahru, Johor, Malaysia*

(Received August 04, 2016, Revised November 27, 2016, Accepted December 11, 2016)

Abstract. This study investigates numerically the behavior of tilted angle shear connectors embedded in solid concrete slabs. Two different tilted angle connectors were used, titled angle with 112.5 and 135 degrees between the angle leg and steel beam flange. A nonlinear finite element model was developed to simulate and validate the experimental push-out tests. Parametric studies were performed to investigate the variations in concrete strength and connector's dimensions. The results indicate that the ultimate strength of a tilted angle shear connector is directly related to the square root of the concrete compressive strength. The effects of variations in the geometry of tilted angle connectors on the shear capacity are discussed in details. Based on the numerical analyses, two equations are proposed to estimate the ultimate capacity of tilted angle shear connectors of 112.5 and 135 degrees in the defined range of parameters.

Keywords: shear connector; composite; tilted angle; push-out test; finite element method

1. Introduction

Shear connectors are an important part of the design of composite beams. An effective connector provides for adequate shear strength for full composite action between the steel beam and concrete (Mirza and Uy 2009, Shariati *et al.* 2015a). In addition, its ductile behaviour can alarm imminent collapse. The ease of construction and economical aspects are also of concern. The search for new connectors that satisfy these criteria continues and innovative developments appear routinely (Yahya Kasim Al-Darzi and Chen 2006). Nowadays, several types of connectors are available such as stud, Perfobond, channel and angle connectors. The angle shear connector provides for shear strength through one leg and resistance against uplift through another leg that acts as a flange. Different instalment techniques of this shear connector, such as C-shaped and L-shaped, have been studied to date (Loh *et al.* 2006, Choi *et al.* 2008, Shariati *et al.* 2012a, 2013, 2014, Khalilian 2013, Khorramian *et al.* 2015). The tilted angle shear connector is a new type of installing angle shear connectors and is being investigated in this paper (see Fig. 1). To estimate the shear resistance of this connector, an experimental investigation was conducted using push-out test. The current information of the shear capacity of shear connectors and also their load–displacement performance are generally obtained from push-out test or full scale tests (Slutter and Driscoll 1965, Maleki 2002, Maleki and Bagheri 2008a, Shariati *et al.* 2012b, 2013, Yan *et al.* 2015).

Analytical procedures that can predict the nonlinear response and the ultimate load capacity of the composite beams are certainly valuable alternatives for such expensive tests. There are numerous researches on finite element (FE) modelling and analysis of composite beams and shear connectors in the literature (Razaqpur and Nofal 1989, Oguejiofor and Hosain 1997, Lam and EI-Lobody 2001, Faella *et al.* 2002, Wang and Chung 2008, Kwak and Hwang 2010, Daie *et al.* 2011, Shariati *et al.* 2012c, Toghroli *et al.* 2014, Khorramian *et al.* 2015, Safa *et al.* 2016, Shah *et al.* 2016, Tahmasbi *et al.* 2016, Toghroli *et al.* 2016). The analytical methods should be verified against selective, well-controlled experimental results (Soltani *et al.* 2016).

There are limited studies available on the FE modeling of the push-out specimens. The primary studies are concentrated on stud shear connectors conducted by Nakajima et al. (Nakajima *et al.* 2003) and Ellobody *et al.* (Ellobody and Dennis 2002, Lam and El-Lobody 2005). A comprehensive finite element study on the behavior of channel shear connectors was conducted by Maleki and Bagheri (2008b) and Maleki and Mahoutian (2009).

In this paper, a finite element model for the tilted angle connector is proposed. The model is validated against the experimental push-out test results. All the components of the push-out test arrangement are modelled in FE environment and linear and nonlinear properties of components are taken into consideration to establish the ultimate strength and load–displacement behaviour of the connector under monotonic loading (Toghroli *et al.* 2014,

∗Corresponding author, Ph.D.
E-mail: shariatimehdi@yahoo.com

http://www.techno-press.org/?journal=scs&subpage=6
ISSN: 1229-9367 (Print), 1598-6233 (Online)

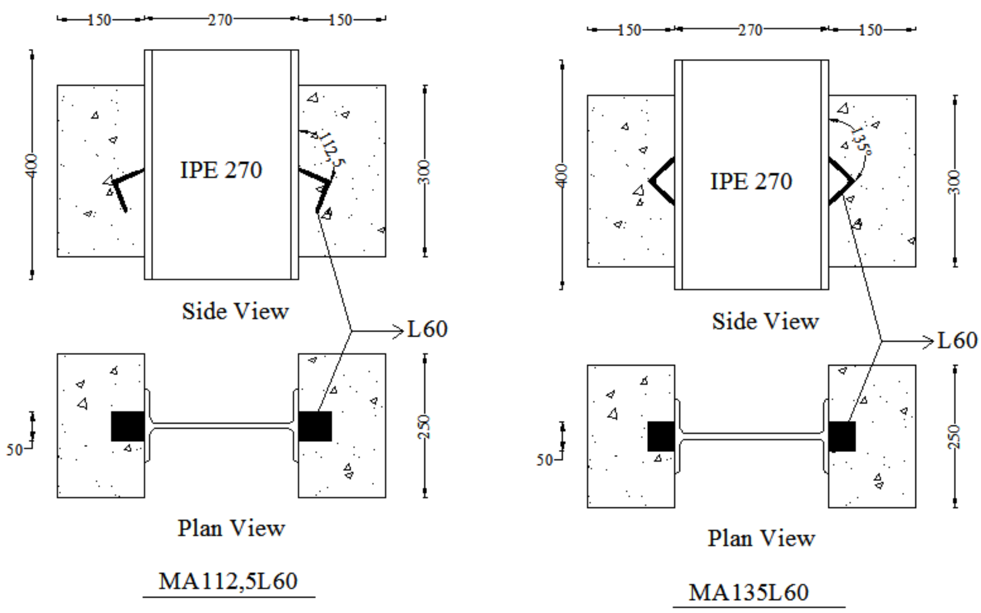

Fig. 1 Schematic presentation of specimens

Table 1 Specimen’s description

No.	Specimen's name	Length (mm)	Tilt angle (degrees)	Angle size	Concrete strength (MPa)
1	MA 112.5 L60	50	112.5	L60×60×6	27.35
2	MA 112.5 L80	50	112.5	L80×80×8	19.44
3	MA 112.5 L100	50	112.5	L100×100×10	26.12
4	MA 135 L60	50	135	L60×60×6	25.48
5	MA 135 L80	50	135	L80×80×8	19.97
6	MA 135 L100	50	135	L100×100×10	31.11
7	MA* 112.5 L80	100	112.5	L80×80×8	25.26
8	MA* 135 L80	100	135	L80×80×8	24.41

Khorramian *et al*. 2015, Safa *et al*. 2016). Furthermore, parametric studies using this model are carried out to investigate the effects of variations in concrete strength and connector dimensions. Finally, two equations are proposed to estimate the ultimate shear capacity of tilted angle shear connectors of 112.5 and 135 degrees in the defined range of parameters.

2. Experimental program

Two types of tilted-shaped angles were tested. The specimens were made by welding two tilted angles to an IPE 270 whose length is 400 mm. The tilted angles were 112.5 and 135 degrees measured with respect to the surface of the attached beam (see Fig. 1). Three different size of angles namely L60, L80, L100 with leg thickness of 6 mm, 8 mm, and 10 mm, respectively were used. Length of angles was 50 mm except L80 for which two different angle length of 50 mm and 100 mm were selected. The angles are embedded in two reinforced concrete blocks on each side with dimensions of 300×250×150 mm.

The maximum nominal aggregate size of 19 mm was used for concrete mix design. The ratio weights of cement, water, sand, gravel were used as 1, 0.42, 2.75, and 1.75 respectively. The 28-day cylindrical compressive strengths of specimens are presented in Table 1. In all specimens, confining steel bars with nominal diameter of 10 mm and yield stress of 300 MPa were used. The only function of confining steel bars was to provide more ductility in concrete blocks and prevent premature failures. Their function was well achieved since observations during test and failure modes showed no crack in concrete but at the interface of steel profile and concrete. The angle shapes showed a good agreement with bilinear stress- strain model. The stress and its corresponding strain at which the slope of stress-strain curves changes are 377.68 MPa and 0.0019 mm/mm, respectively. In addition, the ultimate reported stress and its corresponding strain are 500.73 MPa and 0.2833 mm/mm, respectively.

As it is shown in Fig. 2, the setup of this test is such that the main steel profile is pushed down while the movements of concrete blocks are restricted. Thus, the load transfers directly from the steel beam to the shear connectors. There was a loading cell attached to an actuator as shown in Fig. 2(b). In the test set up, a steel plate was attached to the upper head of the loading machine which applied concentric load to the top of main steel profile. There were two rigid steel supports that provide larger area than concrete block surfaces. Therefore, a uniform load distribution applies on concrete surfaces as reaction. The loading method was displacement control with rate of 0.1 mm/s. The data acquisition system recorded load and displacement of the specimen during each time step. Eight push out tests were performed under monotonic loading by Dartec Universal testing machine, with three different angle sizes. The

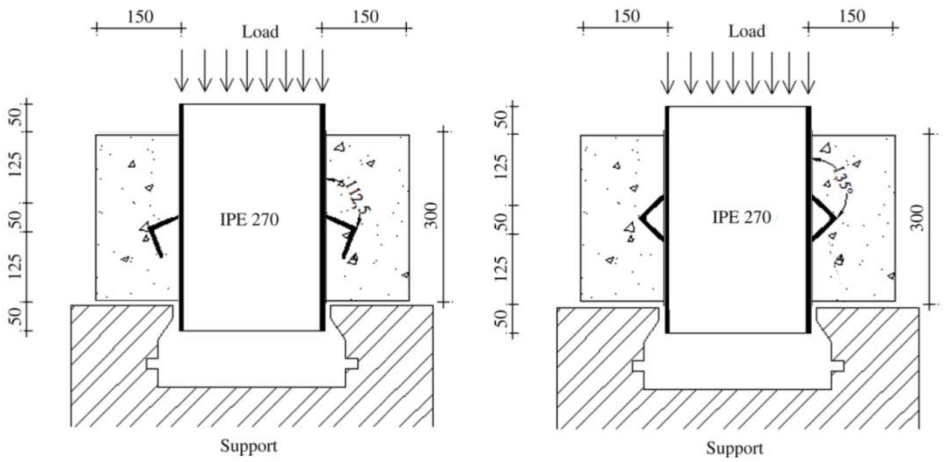

(a)

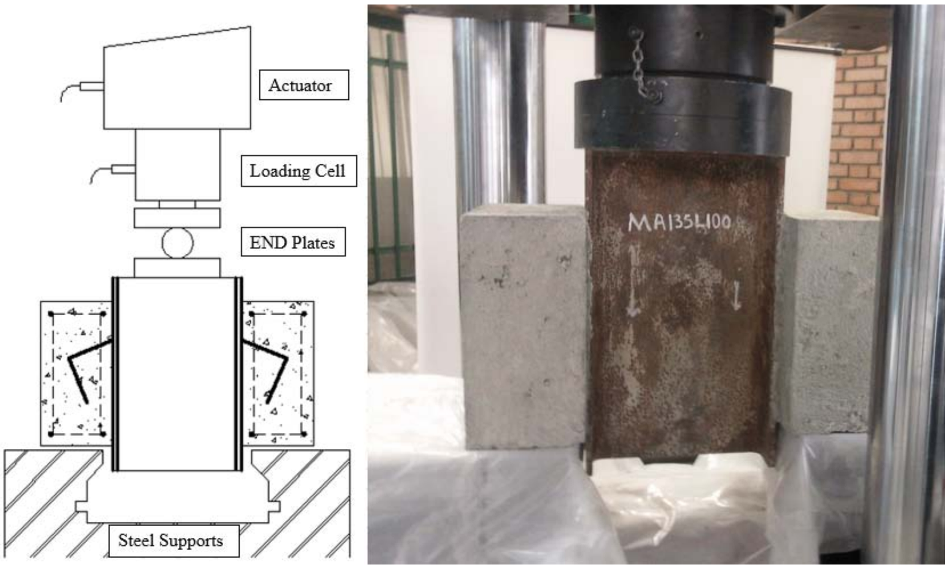

(b)

Fig. 2 (a) Schematic push-out test setup (specimen detail); (b) Push-out test setup detail

specimens are summarized in Table 1. The letter M is used for monotonic loading, A(X) for the tilt angle and L(Y) for the angle size.

3. Finite element model

3.1 General

The finite element program ABAQUS was used to simulate the push-out tests. To reach more accurate results from the FE analysis, all components in the shear connection consisting of concrete slabs, steel beams, rebar and shear connectors were modeled. The static implicit analysis method was employed with stepwise displacement loading.

3.2 Finite element type and mesh

Due to the symmetry of the push-out specimens, only a quarter of the push-out test arrangement with half-length angle connector is modeled. Figs. 3 and 4 show the FE model of a quarter and also a full view of the specimens, respectively.

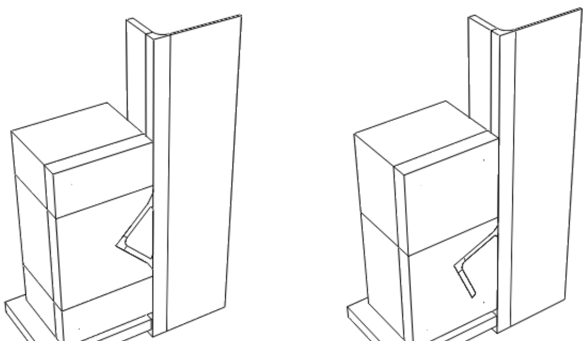

Fig. 3 Quarter of push-out specimens with tilt angle of 135 and 112.5

As indicated in Fig. 5, the concrete slab, shear connector, and steel beam were meshed with solid element C3D8R available in the ABAQUS library. This element is an 8-node brick element with reduced-integration stiffness. Each node

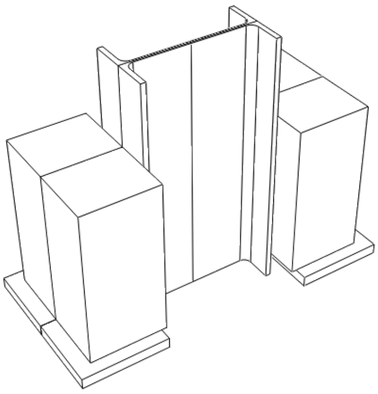

Fig. 4 Full view of push-out specimen

has three translational degrees of freedom. The confining rebar was modeled by the truss element T3D2 which is a 2-node element, and the rigid base was modeled by a 4-node, rigid element R3D4 as presented in Fig. 5. The overall mesh size is about 15 to 12 mm and it was reduced to 4 mm in sensitive places such as interface surfaces, unless a tie constraint was defined in the region.

3.3 Interaction and constraint conditions

As it is shown in Fig. 6, the nodes on the surfaces of the angle-shape around steel beam were tied to the surface of the flange by the tie constraint. Also, frictionless contact interaction was applied to the steel flange and the concrete slab surface. In addition, the contact interaction was used at

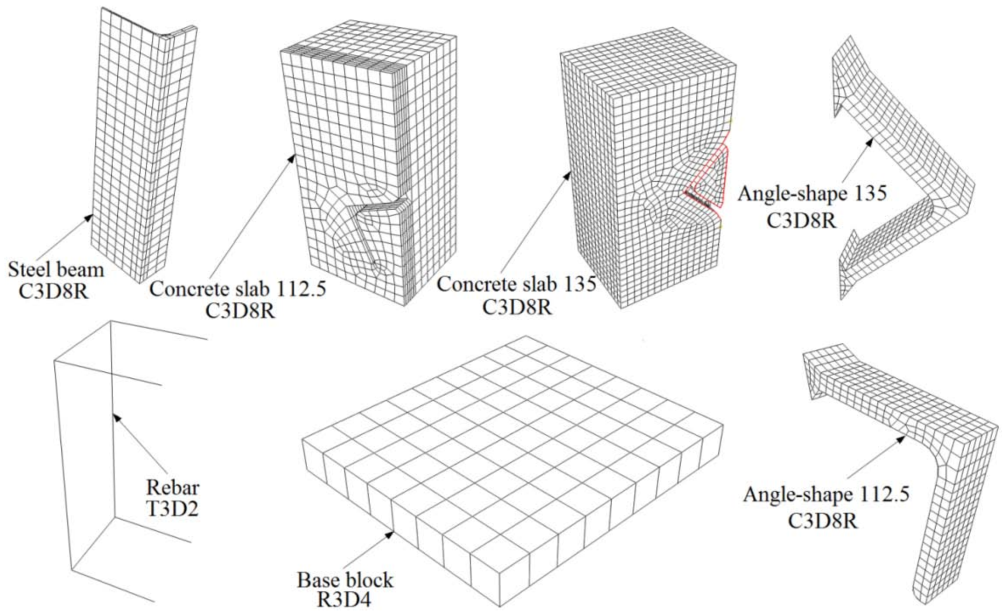

Fig. 5 Finite element type and mesh

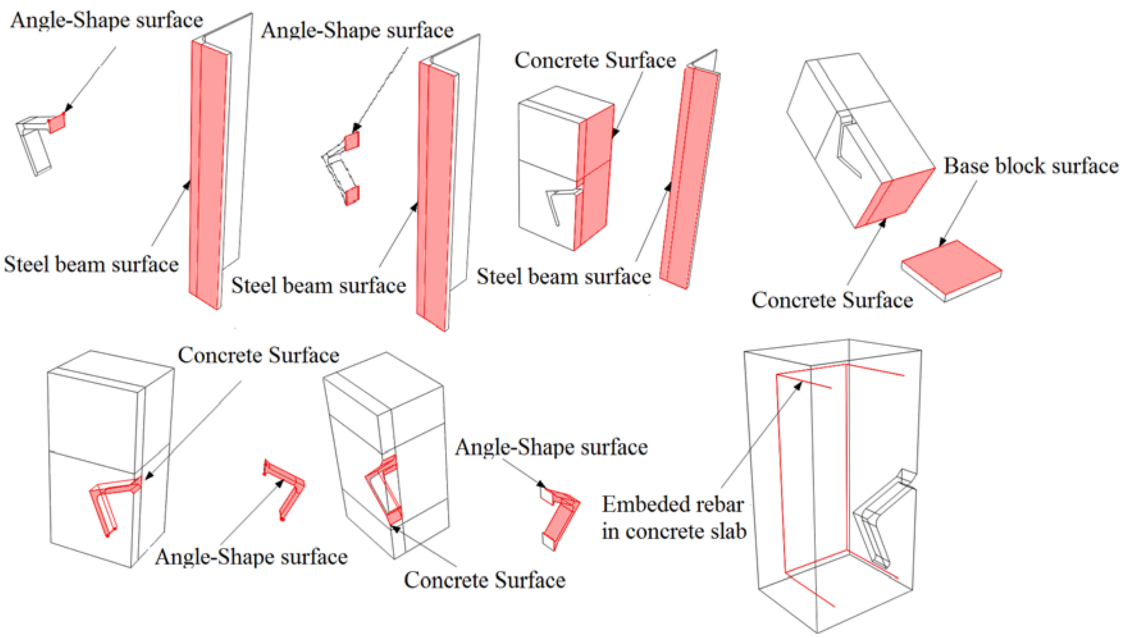

Fig. 6 Constraint and interaction surfaces

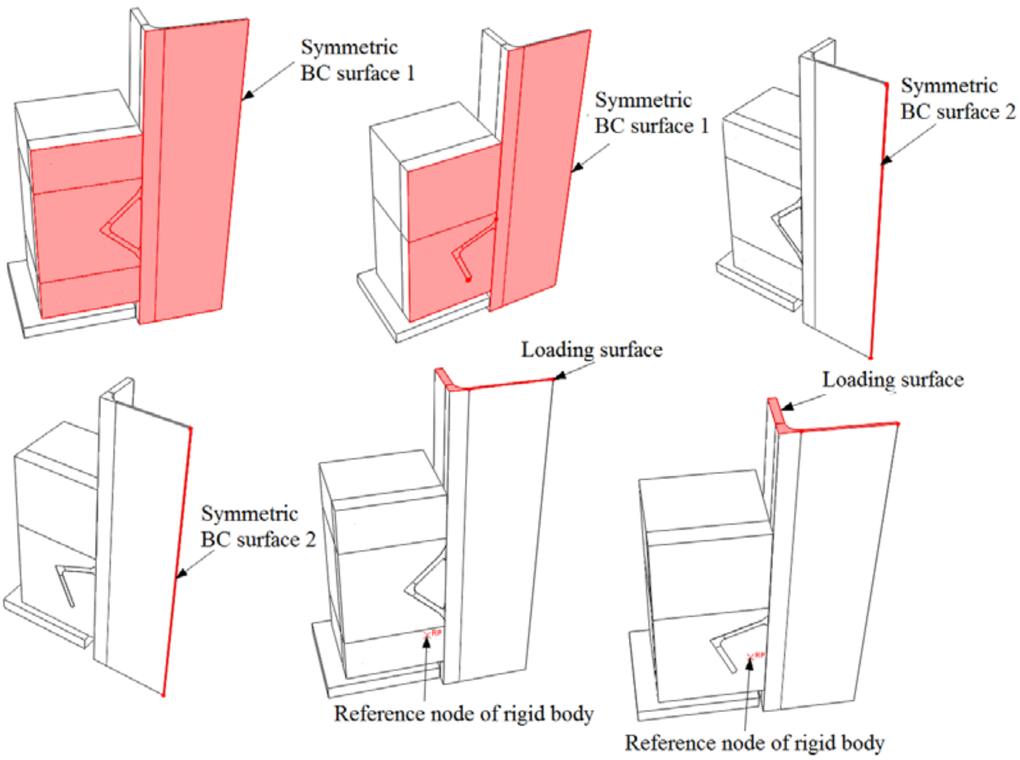

Fig. 7 Boundary condition and loading surfaces

the concrete to angle connector interface by choosing hard contact in normal direction and tangential contact with a friction coefficient of 0.2 with penalty method. Rebar was located inside the concrete slab. The embedded constraint was applied to the rebar and the concrete slab. The interaction between the rigid base and concrete was considered as surface to surface contact. In normal direction ,the interaction was chosen to be hard contact and in tangential direction, penalty method was used. For the sake of accuracy, the model was validated by changing the friction coefficient. Because of using a plastic cover between the concrete slab and rigid base surface in the experimental push-out tests, we observed different friction coefficients on these surfaces for each specimen.Therefore, a coefficient of friction of 0.45 for MA112.5L60 and MA112.5L100, 0.55 for MA112.5L80, 0.7 for MA* 112.5L80, and 0.4 for MA135 specimens were used.

3.4 Loading and boundary conditions

Because of symmetry of the push-out test arrangement, the symmetric boundary condition (BC) was applied to the surfaces at the symmetric planes of the specimen as shown in Fig. 7. The rigid base was assumed to be immovable, so all DOFs of the reference node of the rigid base were restricted. In the analyses, displacement control was applied. Loading was downward and applied as enforced displacement to the top surface of the steel beam.

3.5 Analysis method

In the push-out tests loading were monotonic. Because of the loading increments that are varied very slowly in time; we can neglect the inertia effects. On the other hand,

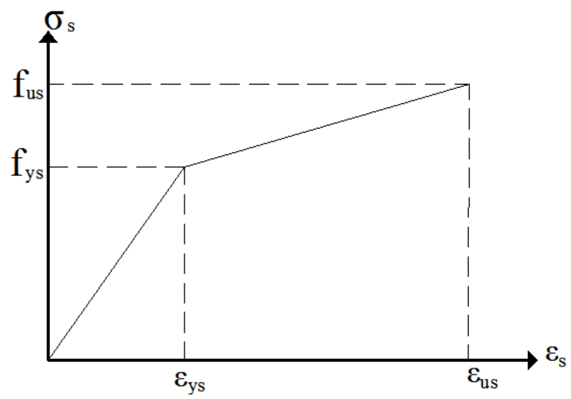

Fig. 8 Schematic stress-strain relationship for steel material

according to ABAQUS User's manual, a static stress analysis is used when inertia effects can be neglected. Therefore, in this study, Static General Method of Analysis was used to obtain accurate results. In addition, the nonlinearity of material, large-displacement effects, and boundary nonlinearitieswere taken into account in these analyses. According to ABAQUS User's manual, Newton's method is used in the mentioned analysis to solve nonlinear equations. The load applies monotonically with a displacement rate of 0.1 mm/s in many increments up to the failure. Thus, as the displacement increases, so does the corresponding load and the software perform an iterative approach to obtain equilibrium in each increment.

3.6 Concrete and steel material properties

Steel material for all parts was modeled by the bilinear curve as shown in Fig. 8. The steel properties are F_y, ε_y, F_u

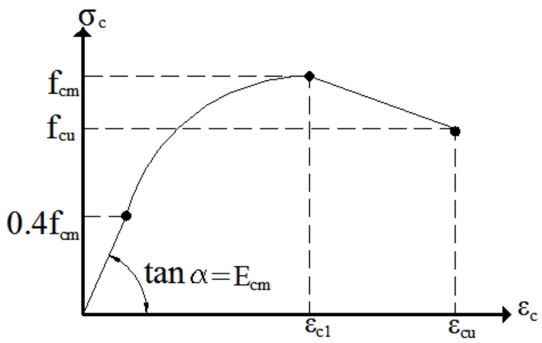

Fig. 9 Schematic stress-strain relationship for concrete material

and εu with the amount of 377.68 MPa, 0.19%, 500.73 MPa and 28.33% respectively.

The nonlinear behavior of concrete material was presented by an equivalent uniaxial stress-strain curve of concrete as shown in Fig. 9. According to EC2 (Institution 2004), the relationship between compression stress and strain was taken as below

$$\sigma_c = \frac{k\eta - \eta^2}{1+(k-2)\eta} f_{cm} \tag{1}$$

$$\eta = \frac{\varepsilon_c}{\varepsilon_{c1}} \tag{2}$$

$$k = 1.05 E_{cm} \frac{\varepsilon_{c1}}{f_{cm}} \tag{3}$$

σ_c = Compression stress(MPa)
k, η = Proportion parameters
E_{cm} = Modulus of elasticity (MPa)
f_{cm} = Ultimate strength of concrete (MPa)
f_{cu} = Compressive Stress corresponding to ε_{cu} (MPa) = $0.85 f_{cm}$
ε_c = Compressive strain of concrete
ε_{cu} = Ultimate strain of concrete = 0.01
ε_{c1} = Strain corresponding to f_{cm} = 0.0022

To define the softening behaviour of concrete when none or small amount of reinforcement is present, the utilization of tension stiffening approach is recommended. The use of stress-strain curve has shown mesh sensitivity. For solving this problem, the fracture energy approach of Hillerborg *et al*. (1976) is utilized. The simplest method is to define tension softening model via linear approximation, in which the linear loss of strength happens after cracking. A more effective technique of defining tension softening is to apply an exponential expression, as experimentally derived by Cornelissen *et al*. (1986). Therefore, in this research, the latter approach with exponential function was used. This study was not covered as such behaviour on advance concrete (Abdul Awal 1988, 1992, Arabnejad *et al*. 2010, 2011, Hossain and Awal 2011, Muhammad *et al*. 2012, Shehu and Awal 2012, Hafizah *et al*. 2014, Muhammad *et al*. 2015, Shariati and Schumacher 2015, 2016, Shariati *et al*. 2015a, Muhammad *et al*. 2016, Walker *et al*. 2016), this will be considered in future research.

Table 2 Plasticity parameters of concrete

Dilation angle	Eccentricity	f_{b0}/f_{c0}	K	Viscosity parameter
45	0.1	1.16	0.666	0

Accordingly, the tension stress with respect to the cracking displacement can be characterized by Eq. (4) (Cornelissen *et al*. 1986).

$$\frac{\sigma_t}{f_t} = f(w) - \frac{w}{w_c} f(w_c) \tag{4}$$

$$f(w) = \left[1 + \left(\frac{c_1 w}{w_c}\right)^2\right] \exp\left(-\frac{c_2 w}{w_c}\right) \tag{5}$$

Where:

f_{cu} = Compressive Stress corresponding to ε_{cu} (MPa) = $0.85 f_{cm}$
f_t = tensile strength of concrete
σ_t = tensile stress of concrete
w = crack opening, mm
w_c = crack opening at which stress cannot be transferred (assumed 0.35 mm in this investigation)
c_1 = material constant and c_1 = 3.0 for normal density concrete
c_2 = material constant and c_2 = 6.93 for normal density concrete

Plasticity parameters of are presented in Table 2. In this study, the compression and tensile damage were used as the following relationships

$$d_t = 1 - \frac{\sigma_t}{f_t} \tag{6}$$

$$d_c = \frac{5\varepsilon_{in}}{5\varepsilon_{in} + 0.01} \tag{7}$$

ε_{in} = Compression inelastic strain

4. Verification of the FE model

In order to verify the proposed finite element model, all push-out specimens were modeled using the assumptions described above. The load-displacement curves for the push-out specimens are shown in Figs. 10 to 17. There is good agreement between experimental and FE results. The maximum loads are compared in Table 3 and Fig. 18.

The von Mises stress contours are presented in Fig. 19 to Fig. 22. The concrete compressive damage at maximum load levels are shown in Figs. 23 and 24. In nearly all cases, the concrete slab was crushed. Thus, a close agreement was observed in all cases between the test results and the FE solution. This proves the adequacy of the FE model in the nonlinear range up to failure.

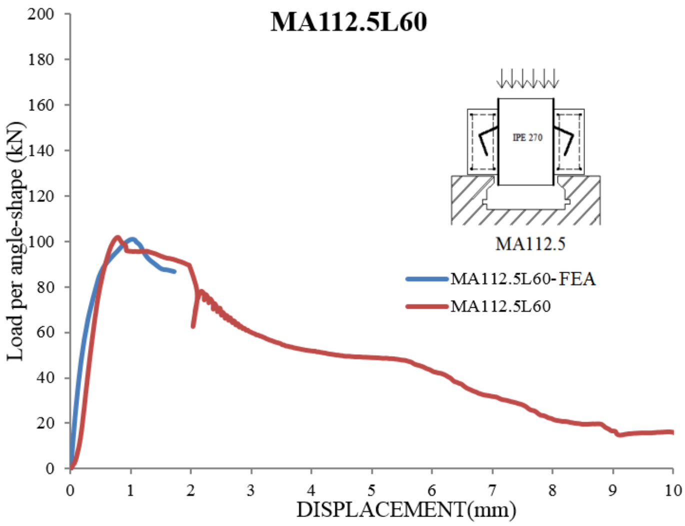

Fig. 10 Load-displacement curves for MA112.5L60; FE analysis vs. test results

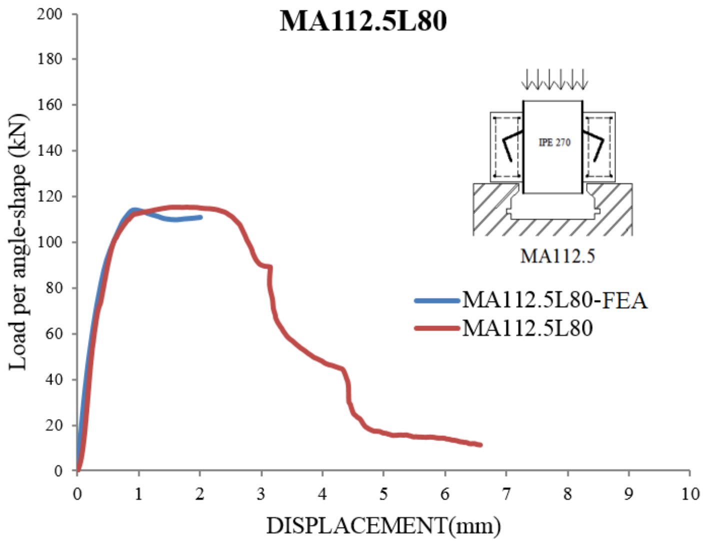

Fig. 11 Load-displacement curves for MA112.5L80; FE analysis vs. test results

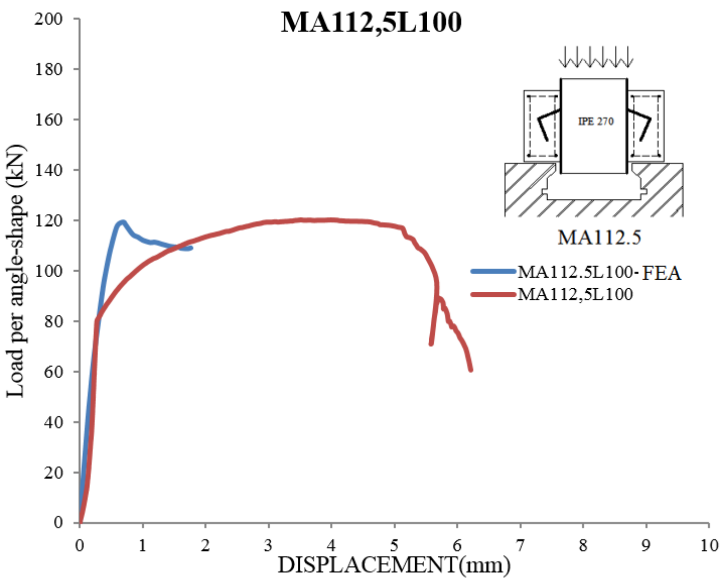

Fig. 12 Load-displacement curves for MA112.5L100; FE analysis vs. test results

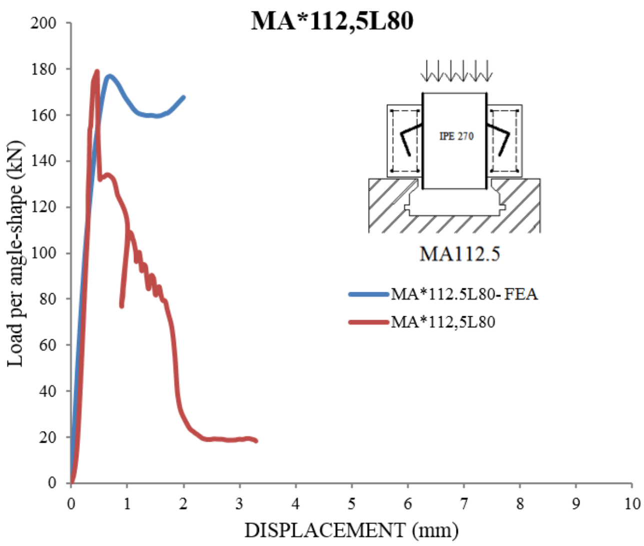

Fig. 13 Load-displacement curves for MA*112.5L80; FE analysis vs. test results

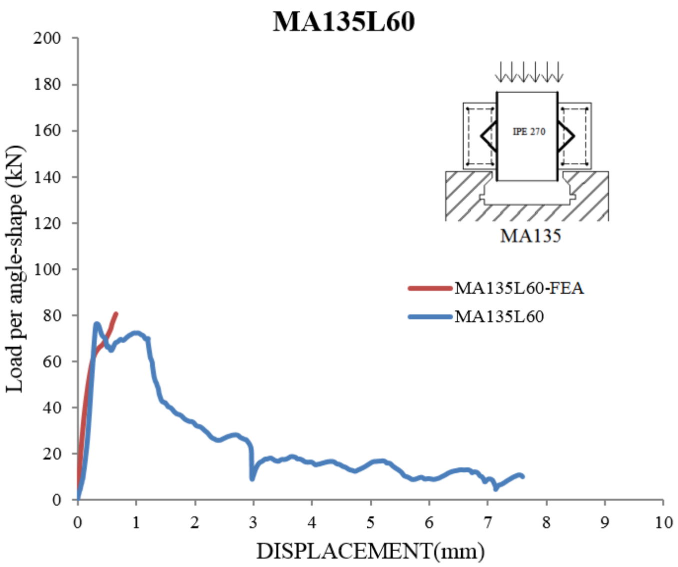

Fig. 14 Load-displacement curves for MA135L60; FE analysis vs. test results

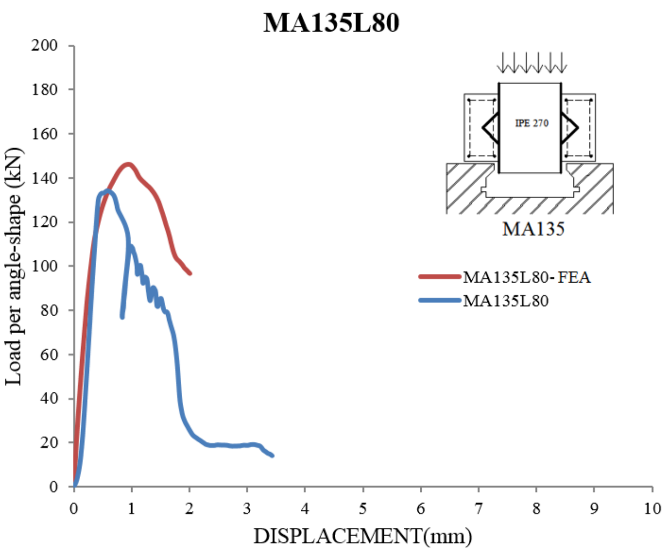

Fig. 15 Load-displacement curves for MA135L80; FE analysis vs. test results

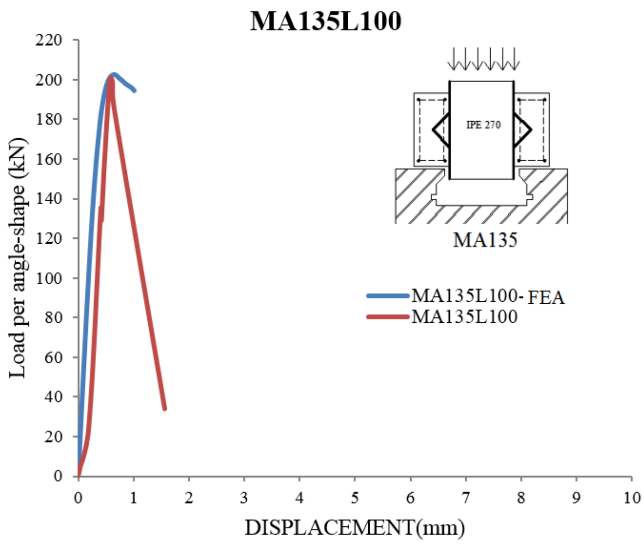

Fig. 16 Load-displacement curves for MA135L100; FE analysis vs. test results

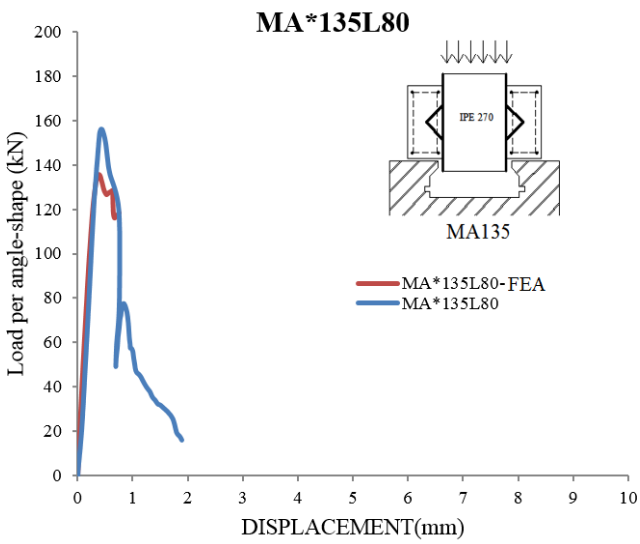

Fig. 17 Load-displacement curves for MA*135L80; FE analysis vs. test results

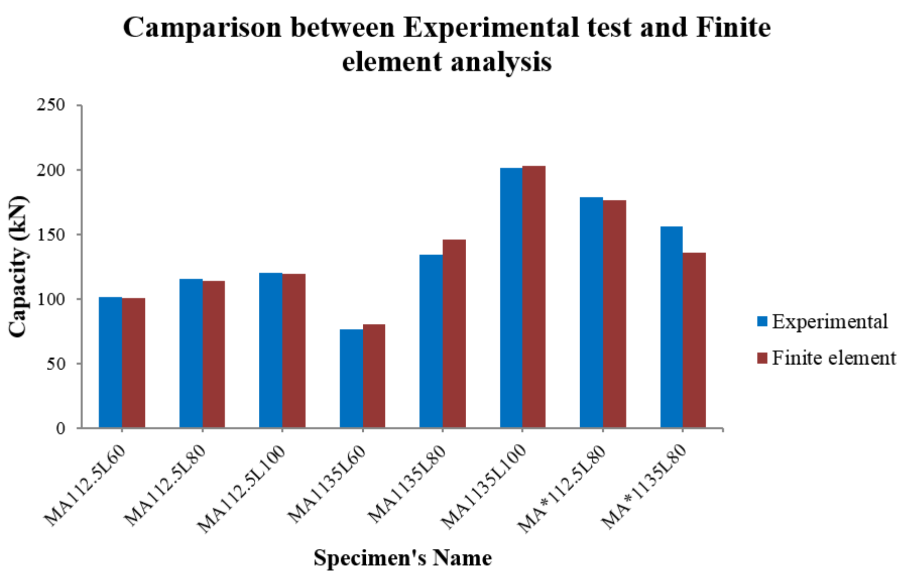

Fig. 18 Load-displacement curves for MA*135L80; FE analysis vs. test results

Table 3 Comparison between experimental tests and finite element analyses

Specimens	Maximum load (kN)	
	Experimental	Finite element
MA112.5L60	101.57	100.99
MA112.5L80	115.41	114.21
MA112.5L100	120.10	119.46
MA135L60	76.36	80.56
MA135L80	134.11	145.93
MA135L100	201.13	202.69
MA*112.5L80	179.04	176.70
MA*135L80	156.18	135.56

5. Parametric studies

Using the FE model that was verified against the test results, a parametric study is conducted here to evaluate the effects of concrete compressive strength, angle dimensions and length of tilted angles of 112.5 and 135 degrees. Summary of the results for the effect of these parameters is given in Tables 4 and 5 for the tilted angle of 112.5 and 153 degrees, respectively. The details are described in the following sections.

5.1 Effect of concrete strength

A parametric study was conducted using the FE model with various concrete compressive cylinder strengths of 20,

Table 4 Results of parametric study for tilted angles of 112.5 degree

No.	L-shape	t (mm)	H (mm)	L (mm)	f_c (MPa)	Max (kN)	Eq. (8)	Error %
1	L50×4	4	50	50	30	92.1127	91.345	0.83
2	L50×5	5	50	50	30	101.488	98.766	2.68
3	L50×6	6	50	50	30	103.552	105.273	1.66
4	L50×7	7	50	50	30	111.048	111.109	0.05
5	L50×8	8	50	50	30	115.901	116.425	0.45
6	L50×9	9	50	50	30	120.519	121.325	0.67
7	L55×5	5	55	50	30	102.532	98.766	3.67
8	L55×6	6	55	50	30	105.363	105.273	0.09
9	L55×8	8	55	50	30	119.829	116.425	2.84
10	L55×10	10	55	50	30	126.435	125.883	0.44
11	L60×5	5	60	50	30	99.8585	98.766	1.09
12	L60×6	6	60	50	20	86.9911	85.955	1.19
13	L60×6	6	60	50	25	97.088	96.101	1.02
14	L60×6	6	60	50	30	104.773	105.273	0.48
15	L60×6	6	60	50	35	110.159	113.708	3.22
16	L60×6	6	60	50	40	115.794	121.559	4.98
17	L60×6	6	60	50	45	119.972	128.933	7.47
18	L60×6	6	60	50	50	123.613	135.907	9.95
19	L60×6	6	60	40	30	101.34	94.581	6.67
20	L60×6	6	60	60	30	110.421	114.902	4.06
21	L60×6	6	60	70	30	117.351	123.726	5.43
22	L60×6	6	60	80	30	123.025	131.916	7.23
23	L60×6	6	60	90	30	129.523	139.588	7.77
24	L60×6	6	60	100	30	140.766	146.829	4.31
25	L60×8	8	60	50	30	115.144	116.425	1.11
26	L60×10	10	60	50	30	125.083	125.883	0.64
27	L65×6	6	65	50	30	107.245	105.273	1.84
28	L65×7	7	65	50	30	109.784	111.109	1.21
29	L65×8	8	65	50	30	113.248	116.425	2.81
30	L65×9	9	65	50	30	117.758	121.325	3.03
31	L65×11	11	65	50	30	128.407	130.153	1.36
32	L70×6	6	70	50	30	107.067	105.273	1.68
33	L70×7	7	70	50	30	109.577	111.109	1.4
34	L70×9	9	70	50	30	118.77	121.325	2.15
35	L70×11	11	70	50	30	121.772	130.153	6.88

Table 4 Continued

No.	L-shape	t (mm)	H (mm)	L (mm)	f_c (MPa)	Max (kN)	Eq. (8)	Error %
36	L75×6	6	75	50	30	107.332	105.273	1.92
37	L75×7	7	75	50	30	110.163	111.109	0.86
38	L75×8	8	75	50	30	112.973	116.425	3.06
39	L75×10	10	75	50	30	121.053	125.883	3.99
40	L75×12	12	75	50	30	128.532	134.177	4.39
41	L80×7	7	80	50	30	110.119	111.109	0.9
42	L80×8	8	80	50	20	95.0092	95.061	0.05
43	L80×8	8	80	50	25	106.183	106.281	0.09
44	L80×8	8	80	50	30	115.441	116.425	0.85
45	L80×8	8	80	50	35	123.63	125.754	1.72
46	L80×8	8	80	50	40	131.198	134.436	2.47
47	L80×8	8	80	50	45	137.463	142.591	3.73
48	L80×8	8	80	50	50	140.989	150.304	6.61
49	L80×8	8	80	40	30	110.164	104.6	5.05
50	L80×8	8	80	60	30	127.337	127.073	0.21
51	L80×8	8	80	70	30	138.125	136.832	0.94
52	L80×8	8	80	80	30	147.872	145.89	1.34
53	L80×8	8	80	90	30	161.328	154.375	4.31
54	L80×8	8	80	100	30	173.598	162.383	6.46
55	L80×10	10	80	50	30	122.913	125.883	2.42
56	L80×12	12	80	50	30	135.433	134.177	0.93
57	L80×14	14	80	50	30	135.456	141.615	4.55
58	L90×8	8	90	50	30	116.206	116.425	0.19
59	L90×9	9	90	50	30	117.737	121.325	3.05
60	L90×11	11	90	50	30	125.949	130.153	3.34
61	L90×13	13	90	50	30	132.879	137.99	3.85
62	L90×16	16	90	50	30	147.766	148.391	0.42
63	L100×8	8	100	50	30	117.639	116.425	1.03
64	L100×10	10	100	50	20	104.867	102.783	1.99
65	L100×10	10	100	50	25	116.793	114.915	1.61
66	L100×10	10	100	50	30	127.037	125.883	0.91
67	L100×10	10	100	50	35	135.304	135.969	0.49
68	L100×10	10	100	50	40	140.032	145.357	3.8
69	L100×10	10	100	50	45	144.771	154.174	6.5
70	L100×10	10	100	50	50	148.121	162.514	9.72
71	L100×10	10	100	40	30	115.203	113.096	1.83
72	L100×10	10	100	60	30	140.557	137.396	2.25
73	L100×10	10	100	70	30	148.399	147.947	0.3
74	L100×10	10	100	80	30	156.228	157.741	0.97
75	L100×10	10	100	90	30	169.739	166.916	1.66
76	L100×10	10	100	100	30	178.1	175.574	1.42
77	L100×12	12	100	50	30	134.768	134.177	0.44
78	L100×14	14	100	50	30	141.838	141.615	0.16
79	L100×16	16	100	50	30	147.794	148.391	0.4
80	L100×20	20	100	50	30	158.355	160.445	1.32
81	L110×10	10	110	50	30	130.301	125.883	3.39
82	L110×12	12	110	50	30	136.459	134.177	1.67

Table 5 Results of parametric study for tilted angles of 135 degree

No.	L-shape	t (mm)	H (mm)	L (mm)	f_c (MPa)	Max (kN)	Eq. (9)	Error %
1	L75×12	12	75	50	30	172.511	179.987	4.33
2	L80×8	8	80	50	20	157.464	151.582	3.74
3	L80×8	8	80	50	25	177.617	169.474	4.58
4	L80×8	8	80	50	30	192.885	185.65	3.75
5	L80×8	8	80	50	35	204.156	200.524	1.78
6	L80×8	8	80	50	40	213.773	214.37	0.28
7	L80×8	8	80	50	45	219.386	227.373	3.64
8	L80×8	8	80	40	30	180.702	196.301	8.63
9	L80×8	8	80	60	30	191.212	177.378	7.23
10	L80×8	8	80	70	30	171.507	170.672	0.49
11	L80×8	8	80	80	30	170.167	165.068	3
12	L80×8	8	80	90	30	148.313	160.279	8.07
13	L80×8	8	80	100	30	138.896	156.112	12.39
14	L80×12	12	80	50	30	193.519	185.65	4.07
15	L80×14	14	80	50	30	195.165	185.65	4.88
16	L90×8	8	90	50	30	193.404	196.448	1.57
17	L90×9	9	90	50	30	194.61	196.448	0.94
18	L90×11	11	90	50	30	195.776	196.448	0.34
19	L90×13	13	90	50	30	199.766	196.448	1.66
20	L90×16	16	90	50	30	203.008	196.448	3.23
21	L100×8	8	100	50	30	194.178	206.638	6.42
22	L100×10	10	100	50	20	165.29	168.719	2.07
23	L100×10	10	100	50	25	182.053	188.634	3.61
24	L100×10	10	100	50	30	197.773	206.638	4.48
25	L100×10	10	100	50	35	211.57	223.195	5.49
26	L100×10	10	100	50	40	222.951	238.605	7.02
27	L100×10	10	100	40	30	193.351	218.493	13
28	L100×10	10	100	60	30	199.514	197.431	1.04
29	L100×10	10	100	70	30	195.231	189.967	2.7
30	L100×10	10	100	80	30	184.869	183.73	0.62
31	L100×10	10	100	90	30	179.732	178.399	0.74
32	L100×10	10	100	100	30	173.596	173.761	0.1
33	L100×12	12	100	50	30	208.048	206.638	0.68
34	L100×14	14	100	50	30	205.964	206.638	0.33
35	L100×16	16	100	50	30	209.001	206.638	1.13
36	L100×20	20	100	50	30	206.44	206.638	0.1
37	L110×10	10	110	50	30	214.745	216.311	0.73
38	L110×12	12	120	50	30	215.105	225.537	4.85
39	L110×14	14	120	50	30	218.731	225.537	3.11
40	L120×11	11	120	50	30	238.996	225.537	5.63
41	L120×12	12	120	50	30	231.652	225.537	2.64
42	L120×13	13	120	50	30	234.033	225.537	3.63
43	L120×15	15	120	50	30	235.341	225.537	4.17

25, 30, 35, 40, 45, and 50 MPa. The other properties of models were kept constant as explained in section 3 and 4. The load-displacement relationships for diverse concrete strengths are presented in Fig. 25 and 26. In these figures, L80×8 have been chosen as a representative of other specimens. It is seen from FE results that the ultimate strength of a tilted angle shear connector is increased as the concrete compressive strength increases for both types of

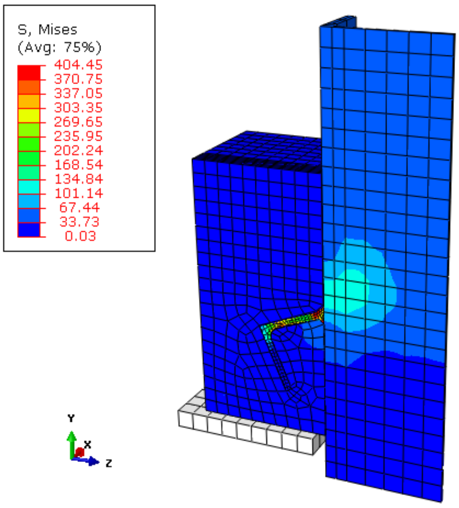

Fig. 19 Stress contour in MA112.5L80 specimen from FE analysis

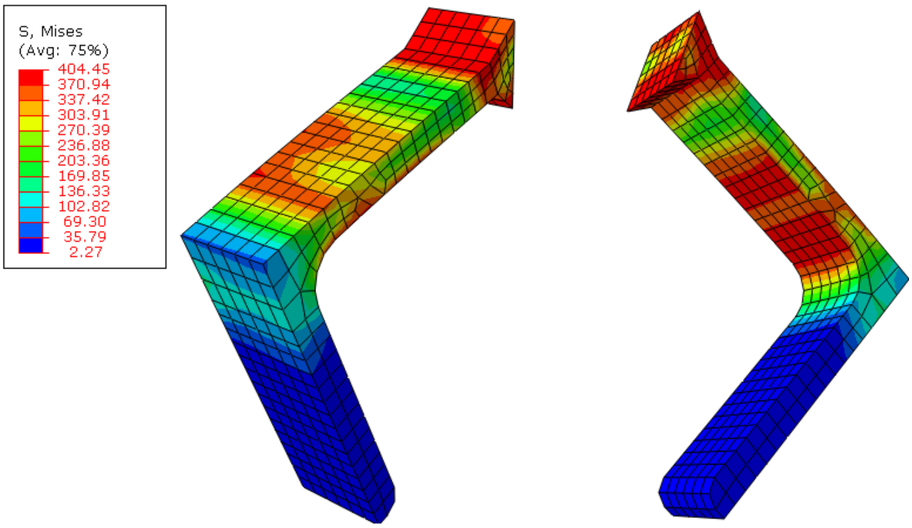

Fig. 20 Stress contour in the angle for MA112.5L80 from FE analysis

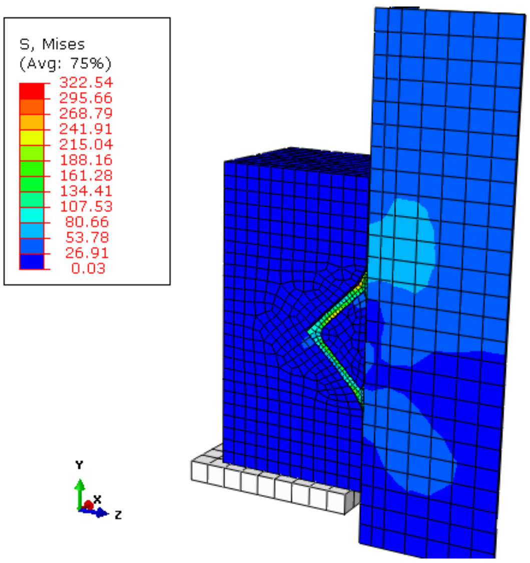

Fig. 21 Stress contour in MA135L80 specimen from FE analysis

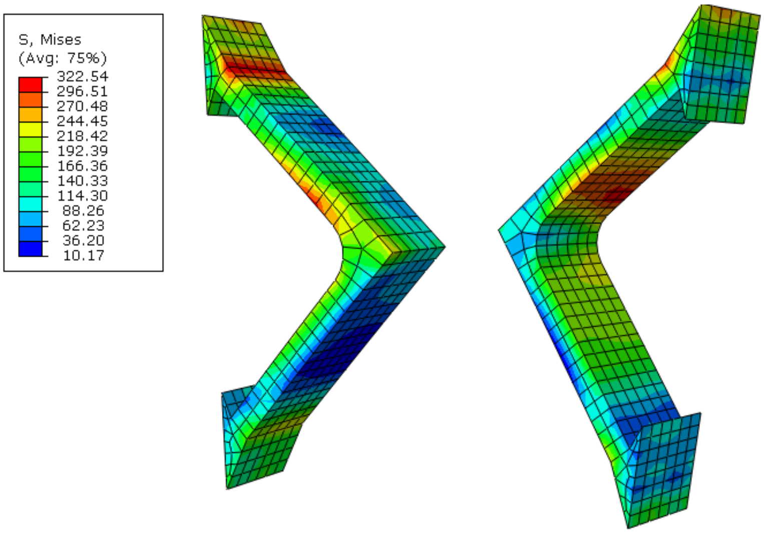

Fig. 22 Stress contour in the angle for MA135L80 from FE analysis

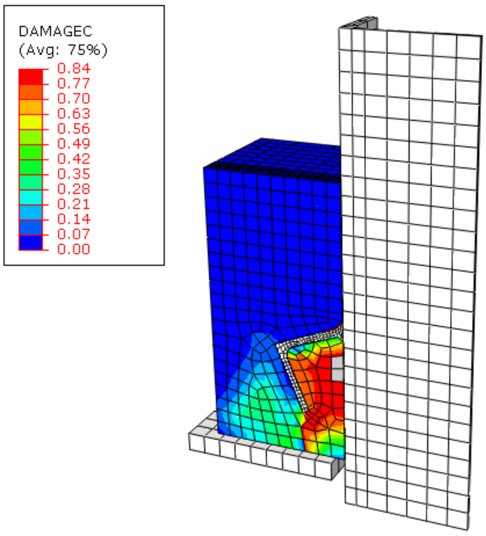

Fig. 23 Compression Damage contour in concrete slab for MA112.5L80 from FE analysis

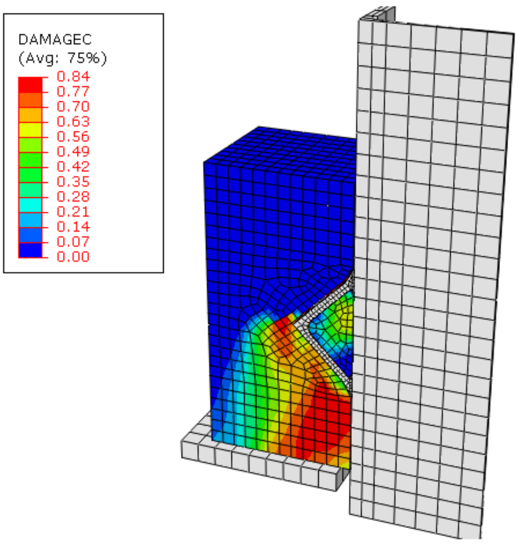

Fig. 24 Compression Damage contour in concrete slab for MA135L80 from FE analysis

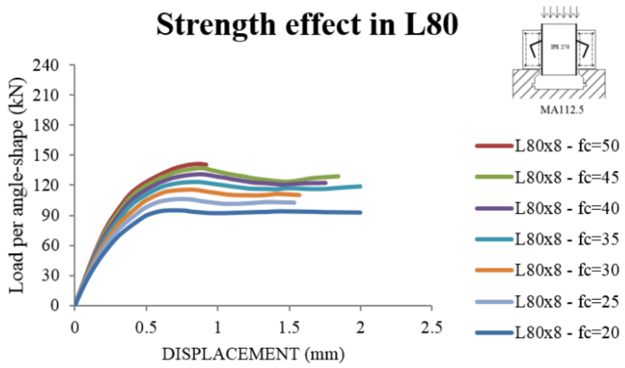

Fig. 25 Load-displacement curves for L80×8 of 112.5 degree with different concrete strength

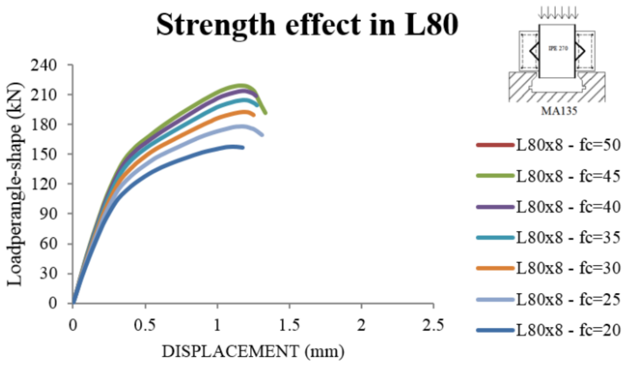

Fig. 26 Load-displacement curves for L80×8 of 135 degrees with different concrete strength

models.

5.2 Effect of angle height

To study the effects of tilted angle height on the ultimate strength, angles with unique thickness and concrete strength of 30 MPa but variable leg sizes were modeled. The angle height of 50, 55, 60, 65, 75, 80 and 100 were studied for the 112.5 degree tilted angle. For the 135 degree tilted angle,

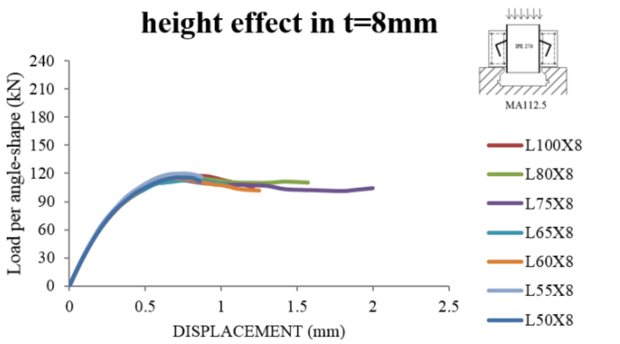

Fig. 27 Load-displacement curves for tilted angle of 112.5 degree with different angle height

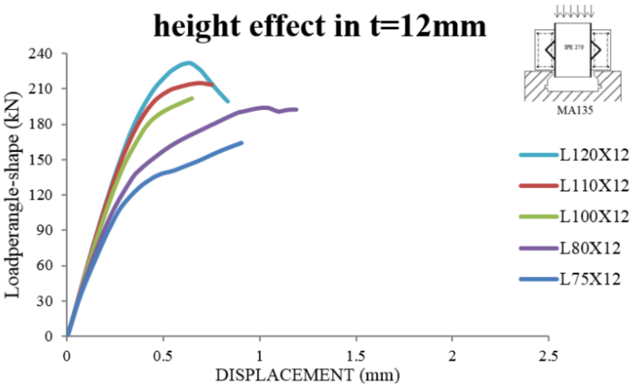

Fig. 28 Load-displacement curves for tilted angle of 135 degrees with different angle height

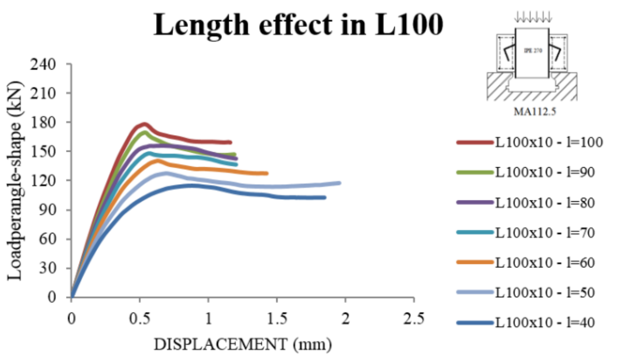

Fig. 29 Load-displacement curves for tilted angle of 112.5 degree with different angle length

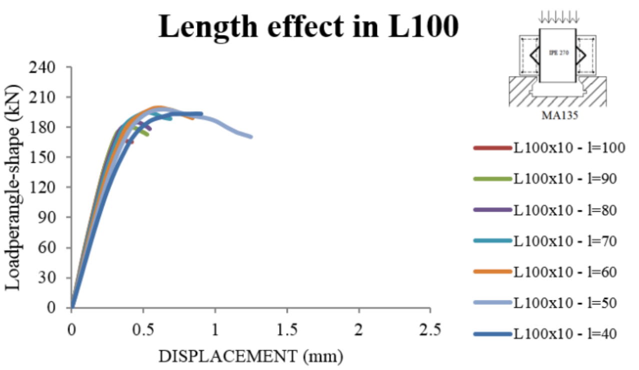

Fig. 30 Load-displacement curves for tilted angle of 135 degrees with different angle length

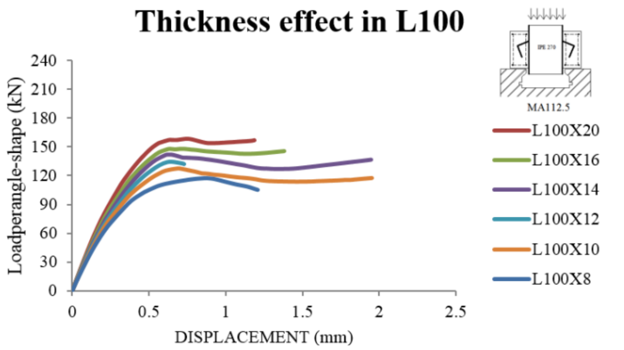

Fig. 31 Load-displacement curves for L100 of 112.5 degree with different leg thickness

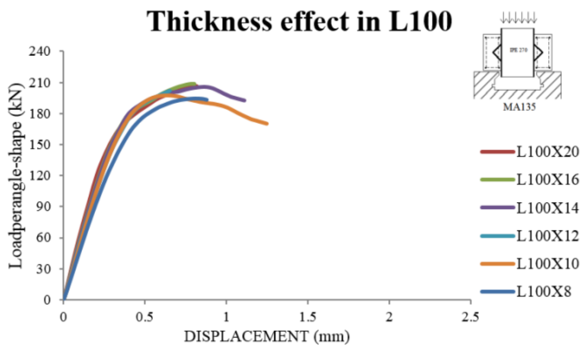

Fig. 32 Load-displacement curves for L100 of 135 degrees with different leg thickness

angle height of 75, 80, 100, 110 and 120 were examined. The results are presented in Figs. 27 and 28. The FE analysis shows that there is an approximately negligible change in ultimate load capacity for models of 112.5 degree when the height changes. For the models of 135 degrees, however, it is observed that by increasing the height of tilted angle, the ultimate capacity increases.

5.3 Effect of angle length

A parametric study was conducted using the FE model with various tilted angle length of 40, 50, 60, 70, 80, 90, and 100 mm. The other properties of models are kept constant as explained in section 3 and 4. The load-displacement relationships for tilted angle of different lengths are presented in Figs. 29 and 30. In these figures, L100×10 was used as the representative of other specimens. According to the FE results, the ultimate strength of tilted angle shear connectors of 112.5-degree increase as the angle length increases. However, for models of 135-degree FE analysis shows reverse effect on ultimate capacity; that means, as the tilted angle length increases, the ultimate shear capacity declined for this type of shear connector.

5.4 Effect of leg thickness

In order to study the effects of leg thickness on the ultimate strength of the tilted angle shear connectors, the results of the FE analysis of L100, as a representative specimen, with concrete strength of 30 MPa and different thicknesses are presented in Figs. 31 and 32. The other properties were kept constant as explained in Sections 3 and 4. As indicated in the figures for tilted angles of 112.5, as the thickness increases, the ultimate shear capacity of the connectors increases while for tilted angles of 135, changing leg thickness has a negligible effect on the ultimate capacity.

5.5 Generating new equation for tilted angles of 112.5 and 135 degrees

Prior researches on angle-shaped shear connectors prove that there is a certain relationship between ultimate strength of shear connector (Q) and product of concrete strength (f_c), thickness of angle (t), height of angle legs (h), and length of angle (L), however each has an unknown power. By using regression on the data that were presented in Table 4, from FE models with various parameters, a new relationship was generated for estimating ultimate shear capacity of tilted angle of 112.5 degree (Eq. (8)). By using the same procedure and data from table 5, another new formula for estimating ultimate shear capacity of tilted angle of 135 degrees with height greater than 80 mm (Eq. (9)) was proposed. There are average errors of 2.6% and 3.6% for models of 112.5 and 135 degrees, respectively, between the FE results and the corresponding equations.

$$Q_{112.5} = 1.57\sqrt{f_c}\,t^{0.35}L^{0.48} \tag{8}$$

$$Q_{135} = 11\sqrt{f_c}\,h^{0.48}L^{-0.25} \tag{9}$$

$Q_{112.5}$ and Q_{135} are the load carrying capacities (in kN) of tilted angle shear connector with tilted angles of 112.5 and 135 degrees, respectively; *h*, *t*, and *L* are the height, the web thickness, and the length of the angle shear connector respectively (mm); f_c is the concrete compressive strength (MPa).

The comparison between experimental results and derived formulas are shown in Table 6. According to this table, it is seen that Eqs. (8) and (9) are predicting the ultimate shear capacity of tilted angles with a relatively good accuracy. However, there are some limitations in predicting the actual shear capacity of these kinds of shear connectors using the proposed equations. The effect of yielding stress of angle shape has not been included in these equations, since the dominant mode of failure is concrete crushing. When crushing of concrete occurs prior to yielding of angle shear connector, the yielding of shear connector has no relevance in determining shear capacity. The latter could be the reason why in similar cases, like C-shape connectors, researchers neglect the effect of yielding of shear connectors.

Table 6 A comparison between experimental results and derived formulas

Specimen	Failure load (kN)	Eq. (8) (kN)	Eq. (9) (kN)	Test/ Eq. (8)	Test/ Eq. (9)
MA112.5L60	101.56	100.52		1.01	
MA112.5L80	115.4	93.72		1.23	
MA12.5L100	120.09	117.46		1.02	
MA135L80	134.11		151.47		0.89
MA135L100	201.13		210.43		0.96
MA*112.5L80	179.04	149		1.2	
MA*135L80	156.18		140.82		1.11

6. Discussion

6.1 Load-displacement behavior

As it is shown in Figs. 10-17, there is a good agreement between finite element results and test results. However, in nearly all cases, the ascending branch is well verified; the slope of ascending branch of load-displacement derived from finite element model as well as the peak load are very compatible and close to the experimental results which shows the strength of the proposed model. In contrary, the descending branch either is not available or does not show a close agreement with experimental results. The reason for the latter problem could be due to the type of numerical analysis that has been performed by finite element software. The software attempts to satisfy equilibrium by iterative procedure over each displacement increment. After failure in concrete happens, excessive strains and stresses occur, the iterative equilibrium approachtries hard to satisfy the equilibrium in the whole model. Eventually, the run of finite element model will be terminated by many iterations without converging as it is observed in Fig. 14. Even if it converges, after a few increments the results are not logical enough as it could be seen in Figs. 11 and 13. However, for other specimens, the descending branch exists and is fairly compatible with the test results although it cannot predict large displacements accurately.

6.2 Modes of failure

As it is illustrated through Figs. 19 and 21, the stress concentration has been observed in both angle shear connectors and IPE beam. For MA112.5 models, as it is presented in Fig. 19, the stress concentration is exactly on the intersection of shear connector and steel beam and the value of stress decreases by moving from the top of flange to the center of web. The shape of this stress contour is like a circle whose center is roughly at the interface of shear connector leg and flange of steel beam. The latter proves that the load is transferring from steel beam to the shear connector which in turn shows a good compatibility of FE model with experimental results. Similarly, for MA135 the same observation could be seen in Fig. 21.

Moreover, Figs. 20 and 21 show the stress distribution contours in tilted angle shear connectors of 112.5 and 135 degrees, respectively. For MA112.5 specimens, the concentration of stress is at the point which is attached to the steel beam. From experimental results, on the other hand, one of the failure modes that has been observed is connector fracture. This fracture shows an extreme stress concentration in interface of angle connector and steel beam. Thus, the finite element model again shows a good agreement to experimental results. The same stress concentration has been observed in MA135, however, these specimens have two legs welded to steel beams as well as extra weld in comparison to MA112.5 specimens. The latter is the reason why the only mode of failure in MA135 specimens is concrete crushing-splitting. In addition to one extra leg welded to IPE beam, another reason why the behavior of these two types of shear connectors are different is that the MA112.5 shear connectors have a cantilever part which prevents movement of concrete. Thus, for these specimens the failure could happen at the point of maximum bending moment which is again the interface of connector and steel beam.

The final observation in terms of stress concentration is on concrete. As it is predicted from experimental test results, the maximum concrete strain and corresponding stress is below the shear connector where the load will go through concrete to the rigid base or reaction point. Since we have loading at top and reaction at bottom of concrete, the maximum stress concentration in concrete, or the compressive concrete damage criteria, is critical at the section just below the shear connector for both MA112.5 and MA135 specimens as it is shown in Figs. 23 and 24, respectively. The model of concrete damage in specimens is in a good agreement with experimental results which shows that the compressive and cracking models well predict the behavior of concrete in accordance with experimental work. In addition, cracks have not been developed longitudinally and at the middle of specimen which means that rebar cage has been modeled in a compatible way.

6.3 The evaluation of derived formulas

The shear capacities of tilted angle shear connectors using the verified finite element model and the derived Eqs. (8) and (9) for MA112.5 and MA135 specimens have been shown in Tables 4 and 5, respectively. For both cases an average of roughly 5% error has been observed which shows a good agreement between the FE results and derived formulas. In addition, the other comparison between the results of derived equations and experimental data is shown in table 6. The ratio of test results to equation 8 is more than one for all cases, and way further than one for MA112.5 L80. Therefore, the proposed formula for MA112.5 specimens conservatively predicts the ultimate shear capacity while this ratio is slightly less than one for MA135 specimens.

7. Conclusions

In this paper, a nonlinear finite element model including damage prediction was developed to simulate the load–displacement behavior of tilted angle shear connectors. Two tilt angles of 112.5 and 135 degrees were considered. The FE model takes into account the linear and nonlinear material properties of concrete and steel angle connector as well as the nonlinearity due to the contact conditions. The FE model was verified against test results and compared well with the results obtained from the experimental push-out tests.

Parametric studies were carried out to investigate the effects of concrete strength and angle sizes on the ultimate shear strength of the tilted angle shear connectors. It was seen from FE results that the ultimate strength of a tilted angle shear connector is directly related to the square root of concrete compressive strength. In addition, the FE results show that as the leg height of tilted angles increases, there is a negligible change in ultimate strength of 112.5 degrees' models but the capacity of 135 degrees' models increases. Moreover, increasing the thickness of angle leg has no effect on 135 degrees' models, but it leads to growth of shear capacity in models of 112.5 degrees. Finally, as the length of tilted angles increases, the ultimate capacity of models of 112.5 degrees increases while it decreases for the models of 135 degrees. This decline in capacity, for models of 135 degrees, have been observed in models in the range of L80 to L120 with 40 to 100 mm length of tilted angles that can be considered as a limitation for the derived formula for MA135 type.

By using FE analysis results and regression, two equations were proposed to estimate the ultimate capacity of tilted angle shear connectors of 112.5 and 135 degrees in the defined range of parameters with the discussed limitations.

Acknowledgments

The authors would like to acknowledge the support from the Faculty of Civil Engineering, University of Tabriz, Iran, under the Grant No. 102-2500.

References

Abdul Awal, A.S. (1988), "Failure mechanism of prepacked concrete", *J. Struct. Eng.*, **114**(3), 727-732.

Abdul Awal, A.S. (1992), "Creep recovery of prepacked aggregate concrete", *J. Mater. Civil Eng.*, **4**(3), 320-325.

Arabnejad Khanouki, M.M., Ramli Sulong, N.H. and Shariati, M. (2010), "Investigation of seismic behaviour of composite structures with concrete filled square steel tubular (CFSST) column by push-over and time-history analyses", *Proceedings of the 4th International Conference on Steel and Composite Structures*, Sydney, Australia, July.

Arabnejad Khanouki, M.M., Ramli Sulong, N.H. and Shariati, M. (2011), "Behavior of through beam connections composed of CFSST columns and steel beams by finite element studying", *Adv. Mater. Res.*, **168**, 2329-2333.

Choi, S.M., Tateishi, K., Uchida, D., Asano, K. and Kobayashi, K. (2008), "Fatigue strength of angle shape shear connector used in steel-concrete composite slab", *Int. J. Steel Struct.*, **8**(3), 199-204.

Cornelissen, H., Hordijk, D. and Reinhardt, H. (1986), "Experimental determination of crack softening characteristics of normalweight and lightweight concrete", *HERON*, **31**(2), 1986.

Daie, M., Jalali, A., Suhatril, M., Shariati, M., Arabnejad, Khanouki, M.M., Shariati, A. and Kazemi Arbat, P. (2011), "A new finite element investigation on pre-bent steel strips as damper for vibration control", *Int. J. Phys. Sci.*, **6**(36), 8044-8050.

Ellobody, E. and, Lam, D. (2002), "Modeling of headed stud in steel-precast composite beams", *Steel Compos. Struct., Int. J.*,

2(5), 355-378.

Faella, C., Martinelli, E. and Nigro, E. (2002), "Steel and concrete composite beams with flexible shear connection: "exact" analytical expression of the stiffness matrix and applications", *Comput. Struct.*, **80**(11), 1001-1009.

Hafizah, N.A.K., Bhutta, M.A.R., Jamaludin, M.Y., Warid, M.H., Ismail, M., Rahman, M.S., Yunus, I. and Azman, M. (2014), "Kenaf fiber reinforced polymer composites for strengthening RC beams", *J. Adv. Concrete Technol.*, **12**(6), 167-177.

Hillerborg, A., Modéer, M. and Petersson, P.-E. (1976), "Analysis of crack formation and crack growth in concrete by means of fracture mechanics and finite elements", *Cement Concrete Res.*, **6**(6), 773-781.

Hossain, M. and Awal, A.A. (2011), "Experimental validation of a theoretical model for flexural modulus of elasticity of thin cement composite", *Construct. Build. Mater.*, **25**(3), 1460-1465.

Institution, B.S. (2004), Eurocode 2: Design of Concrete Structures: Part 1-1: General Rules and Rules for Buildings, British Standards Institution.

Khalilian, M. (2013), "The assessment of shear capacity of angle shear connectors", Master; Sharif University of Technology.

Khorramian, K., Maleki, S., Shariati, M. and Ramli Sulong, N.H. (2015), "Behavior of tilted angle shear connectors", *PLoS ONE*, **10**(12), e0144288.

Kwak, H.-G. and Hwang, J.-W. (2010), "FE model to simulate bond-slip behavior in composite concrete beam bridges", *Comput. Struct.*, **88**(17-18), 973-984.

Lam, D. and EI-Lobody, E. (2001), "Finite element modelling of headed stud shear connectors in steel-concrete composite beam", Elsevier Science Ltd.

Lam, D. and El-Lobody, E. (2005), "Behavior of headed stud shear connectors in composite beam", *J. Struct. Eng.*, **131**, 96-107.

Loh, H., Uy, B. and Bradford, M. (2006), "The effects of partial shear connection in composite flush end plate joints Part I--experimental study", *J. Construct. Steel Res.*, **62**(4), 378-390.

Maleki, S. (2002), "Effect of deck and support stiffness on seismic response of slab-girder bridges", *Eng. Struct.*, **24**(2), 219-226.

Maleki, S. and Bagheri, S. (2008a), "Behavior of channel shear connectors, Part I: Experimental study", *J. Construct. Steel Res.*, **64**(12), 1333-1340.

Maleki, S. and Bagheri, S. (2008b), "Behavior of channel shear connectors, Part II: Analytical study", *J. Construct. Steel Res.*, **64**(12), 1341-1348.

Maleki, S. and Mahoutian, M. (2009), "Experimental and analytical study on channel shear connectors in fiber-reinforced concrete", *J. Construct. Steel Res.*, **65**(8-9), 1787-1793.

Mirza, O. and Uy, B. (2009), "Behaviour of headed stud shear connectors for composite steel–concrete beams at elevated temperatures", *J. Construct. Steel Res.*, **65**(3), 662-674.

Muhammad, B., Ismail, M., Bhutta, M.A.R. and Abdul-Majid, Z. (2012), "Influence of non-hydrocarbon substances on the compressive strength of natural rubber latex-modified concrete", *Construct. Build. Mater.*, **27**(1), 241-246.

Muhammad, N.Z., Keyvanfar, A., Majid, M.Z.A., Shafaghat, A. and Mirza, J. (2015), "Waterproof performance of concrete: A critical review on implemented approaches", *Construct. Build. Mater.*, **101**, 80-90.

Muhammad, N.Z., Shafaghat, A., Keyvanfar, A., Majid, M.Z.A., Ghoshal, S., Yasouj, S.E.M., Ganiyu, A.A., Kouchaksaraei, M.S., Kamyab, H. and Taheri, M.M. (2016), "Tests and methods of evaluating the self-healing efficiency of concrete: A review", *Construct. Build. Mater.*, **112**, 1123-1132.

Nakajima, A., Saiki, I., Kokai, M., Doi, K., Takabayashi, Y. and Ooe, H. (2003), "Cyclic shear force-slip behavior of studs under alternating and pulsating load condition", *Eng. Struct.*, **25**(5), 537-545.

Oguejiofor, E. and Hosain, M. (1997), "Numerical analysis of push-out specimens with perfobond rib connectors", *Comput. Struct.*, **62**(4), 617-624.

Razaqpur, A.G. and Nofal, M. (1989), "A finite element for modelling the nonlinear behavior of shear connectors in composite structures", *Comput. Struct.*, **32**(1), 169-174.

Safa, M., Shariati, M., Ibrahim, Z., Toghroli, A., Baharom, S.B., Nor, N.M. and Petković, D. (2016), "Potential of adaptive neuro fuzzy inference system for evaluating the factors affecting steel-concrete composite beam's shear strength", *Steel Compos. Struct., Int. J.*, **21**(3), 679-688.

Shah, S., Sulong, N.R., Shariati, M., Khan, R. and Jumaat, M. (2016), "Behavior of steel pallet rack beam-to-column connections at elevated temperatures", *Thin-Wall. Struct.*, **106**, 471-483.

Shariati, A. and Schumacher, T. (2015), "Oversampling in virtual visual sensors as a means to recover higher modes of vibration, 41st Annual Review of Progress in Quantitative Nondestructive Evaluation, Volume 34, AIP Publishing.

Shariati, A. and Schumacher, T. (2016), "Eulerian-based virtual visual sensors to measure dynamic displacements with subpixel accuracy of structures and mechanical systems", *J. Struct. Control Health Monitor*.

Shariati, M., Ramli Sulong, N.H. and Arabnejad Khanouki, M.M. (2012a), "Experimental assessment of channel shear connectors under monotonic and fully reversed cyclic loading in high strength concrete", *Mater. Des.*, **34**, 325-331.

Shariati, M., Ramli Sulong, N.H., Suhatril, M., Shariati, A., Arabnejad, M.M.K. and Sinaei, H. (2012b), "Behaviour of C-shaped angle shear connectors under monotonic and fully reversed cyclic loading: An experimental study", *Mater. Des.*, **41**, 67-73.

Shariati, M., Ramli Sulong, N., Suhatril, M., Shariati A., Arabnejad Khanouki, M. and Sinaei, H. (2012c), "Fatigue energy dissipation and failure analysis of channel shear connector embedded in the lightweight aggregate concrete in composite bridge girders", *Proceedings of the 5th International Conference on Engineering Failure Analysis*, The Hague, The Netherlands, July.

Shariati, M., Ramli Sulong, N.H., Suhatril, M., Shariati, A., Arabnejad Khanouki, M.M. and Sinaei, H. (2013), "Comparison of behaviour between channel and angle shear connectors under monotonic and fully reversed cyclic loading", *Construct. Build. Mater.*, **38**, 582-593.

Shariati, A., Shariati, M., Ramli Sulong, N.H., Suhatril, M., Arabnejad Khanouki, M.M. and Mahoutian, M. (2014), "Experimental assessment of angle shear connectors under monotonic and fully reversed cyclic loading in high strength concrete", *Construct. Build. Mater.*, **52**, 276-283.

Shariati, M., Ramli Sulong, N.H., Shariati, A. and Khanouki, M.A. (2015a), "Behavior of V-shaped angle shear connectors: experimental and parametric study", *Mater. Struct.*, 1-18.

Shariati, A., Schumacher, T. and Ramanna, N. (2015b), "Eulerian-based virtual visual sensors to detect natural frequencies of structures", *J. Civil Struct. Health Monitor.*, **5**(4), 457-468.

Shehu, I. and Awal, A. (2012), "Mechanical properties of concrete incorporating high volume palm oil fuel ash", *Adv. Mater. Res.*, **599**, Trans Tech Publications.

Slutter, R. and Driscoll, G.C. (1965), "Flexural strength of steel and concrete composite beams", *J. Struct. Eng., ASCE*, 71-99.

Soltani, M., Topa, A., Karim, M.R. and Sulong, N.R. (2016), "Crashworthiness of G4 (2W) guardrail system: a finite element parametric study", *Int. J. Crashworth.*, 1-21.

Tahmasbi, F., Maleki, S., Shariati, M., Ramli Sulong, N.H. and Tahir, M.M. (2016), "Shear capacity of C-shaped and L-shaped angle shear connectors", *PLOS ONE*, **11**(8), e0156989.

Toghroli, A., Suhatril, M., Ibrahim, Z., Safa, M., Shariati M. and Shamshirband, S. (2016), "Potential of soft computing approach for evaluating the factors affecting the capacity of steel–concrete composite beam", *J. Intel. Manuf.*, 1-9.

Toghrolia, A., Mohammadhassani, M., Shariatib, M., Suhatrilc, M., Ibrahimd, Z. and Sulong, N.H.R. (2014), "Prediction of shear capacity of channel shear connectors using the ANFIS model", *Steel Compos. Struct., Int. J.,* **17**(5), 623-639.

Walker, C., Miller, T., Gupta, R., Shariati, A. and Schumacher, T. (2016), "Development of virtual visual sensors applications to wood structural health monitoring", *ASTM J. Test. Eval*.

Wang, A.J. and Chung, K.F. (2008), "Advanced finite element modelling of perforated composite beams with flexible shear connectors", *Eng. Struct.*, **30**(10), 2724-2738.

Yahya Kasim Al-Darzi, S. and Chen, A. (2006), "Development of hybrid bridges: State of arts and conceptual design", *J. Appl. Sci.*, **6**(13), 2799-2803.

Yan, J.-B., Liew, J.R., Zhang, M.-H. and Sohel, K. (2015), "Experimental and analytical study on ultimate strength behavior of steel–concrete–steel sandwich composite beam structures", *Mater. Struct.*, **48**(5), 1523-1544.

BU